

Novel and Effective Pyridyl Substituted 1, 2, 4-Triazole as Corrosion Inhibitor for Mild Steel in Acid Solution

K.R Ansari¹, Dileep Kumar Yadav¹, Eno E. Ebenso², M.A. Quraishi^{1,*}

¹ Department of Applied Chemistry, Institute of Technology, Banaras Hindu University, Varanasi 221005, India

² Department of Chemistry, School of Mathematical and Physical Sciences, North-West University (Mafikeng Campus), Private Bag X2046, Mmabatho 2735, South Africa

*E-mail: maquraishi@rediffmail.com

Received: 24 March 2012 / Accepted: 18 April 2012 / Published: 1 May 2012

The corrosion inhibition effect of 4-amino-5-(pyridin-4-yl)-4H-1,2,4-triazol-3-thiol (APTT) was evaluated for mild steel in 1M HCl solution using gravimetric measurement, potentiodynamic polarization and electrochemical impedance spectroscopy (EIS). Inhibition efficiencies obtained ranged between 54.3 to 95.7% in the concentration range of 50 to 200 mgL⁻¹. Double layer capacitance, C_{dl} , and charge transfer resistance, R_{ct} , values were evaluated and discussed. Potentiodynamic polarization study clearly revealed the fact that APTT is a mixed-type inhibitor. The values of activation energy (E_a), adsorption equilibrium constant (ΔK_{ads}), free energy of adsorption (ΔG_{ads}), enthalpy of adsorption (ΔH_{ads}) and entropy of adsorption (ΔS_{ads}) were evaluated to corroborate the mechanism of inhibition. Langmuir adsorption isotherm was found to confirm the adsorption characteristics of inhibitor. Scanning electron microscopy (SEM) and energy dispersive X-ray spectroscopy (EDX) examinations of metal surface confirmed the existence of thin protective film of inhibitor on metal surface.

Keywords: Corrosion inhibition; Gravimetric measurement; EIS; Adsorption; Mild steel; SEM-EDX

1. INTRODUCTION

Mild steel is extensively used in numerous industrial and engineering applications, including construction and designs, where they are deployed in various service environments containing acids, alkali's and salt solutions. These service environments readily lead to inevitable corrosion of exposed surfaces of the metal because of their aggressive nature. It is a general consensus that the best method to protect the metal deployed in these corrosive environments is to add corrosion inhibitors [1].

The use of organic compounds to inhibit corrosion of mild steel has assumed great significance due to their application in preventing corrosion under various corrosive environments. A variety of organic compounds have been reported to be effective as corrosion inhibitors [2]. Most of the effective and efficient organic inhibitors were those compounds that had π - bonds and contained hetero-atoms such as oxygen, nitrogen and sulphur, and phosphorus which allowed adsorption on the metal surface. The organic inhibitors function through adsorption on the metal surface blocking the active sites by displacing water molecules and forming a compact barrier film to decrease the corrosion rate [3].

Due to increasing environmental awareness and adverse effect of some chemicals, research activities in recent times are geared towards developing cheap and environmentally acceptable corrosion inhibitors. As a potential chemotherapeutic and pharmacotherapeutic agent [4], 4-amino-5-(pyridin-4-yl)-4H-1,2,4-triazol-3-thiol (APTT) was found to be a heterocyclic compound containing N, S, and aromatic rings with several π - bonds which could possibly serve as active sites for the adsorption process. To the best of our knowledge APTT has not been used as corrosion inhibitor.

The aim of this work is to investigate the inhibition effect of 4-amino-5-(pyridin-4-yl)-4H-1,2,4-triazol-3-thiol on the corrosion of mild steel in 1M HCl solution by using gravimetric method, electrochemical techniques and surface morphological studies.

2. EXPERIMENTAL

2.1. Chemicals

APTT was synthesized in laboratory according to the methods described elsewhere [4] and its purity was identified by thin layer chromatography (TLC). Melting point was determined in open capillaries and matched with literature. The molecular structure is shown in Fig. 1.

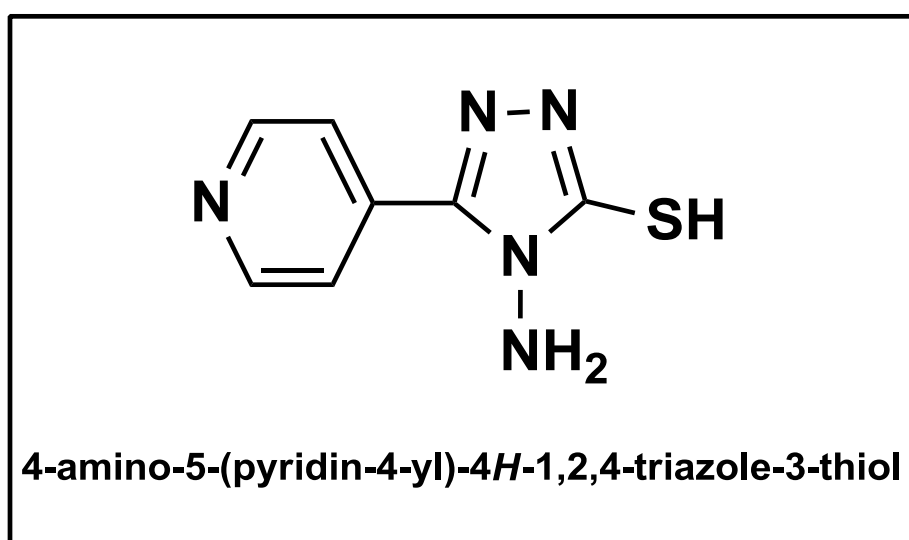


Figure 1. Molecular structure of APTT

2.2. Materials and electrolyte

Corrosion tests were performed on mild steel coupons of following composition (wt %): C = 0.076, Mn = 0.192, P = 0.012, Si = 0.026, Cr = 0.050, Al = 0.023 and balance Fe. Mild steel coupons used in gravimetric and electrochemical experiments were mechanically cut in to $2.5 \times 2 \times 0.025$ and $8 \times 1 \times 0.025$ cm dimensions, and then abraded with SiC abrasive papers of grade 600-1200 respectively, degreased with acetone and dried at ambient temperature. The test solution, 1M HCl was prepared by dilution of analytical grade 37 % HCl with double distilled water. Stock solution of APTT was made by dissolving 100 mg APTT in 100 ml HCl. The concentration of stock solutions was 1000 mg L^{-1} . The concentration range of APTT employed was 50-200 mg L^{-1} .

2.3. Electrochemical measurements

The electrochemical experiments were carried out using a conventional three-electrode cell assembly at ambient temperature. Mild steel coupons of 1 cm^2 area exposed was used as working electrode, platinum foil of 1 cm^2 dimension was used as counter electrode and a saturated calomel electrode (SCE) was used as reference electrode. All experiments were performed in the absence and presence of different concentrations of inhibitor. All electrochemical measurements were carried out using a Gamry Potentiostat /Galvanostat (Model G-300) connected with a personal computer with EIS software Gamry Instruments Inc., USA. The electrochemical experiments were analyzed by electrochemical software Echem Analyst 5.0 software package. All the experiments were measured after immersion of mild steel for 30 min in 1M HCl in absence and presence of inhibitor. Prior to polarization and EIS experiment the electrode was allowed to corrode freely and its open circuit potential (OCP) was recorded as a function of time for 200 seconds. After this time a steady-state OCP corresponding to the corrosion potential (E_{corr}) of the working electrode was obtained.

Potentiodynamic current-potential curves were obtained by changing the electrode potential automatically from -250 up to +250 mV_{SCE} versus OCP at a scan rate of 1 mVs^{-1} . The linear Tafel segments of anodic and cathodic curves were extrapolated to corrosion potential to obtain corrosion current densities (I_{corr}).

Impedance measurements were carried out using AC signals of amplitude 10 mV peak to peak at the open circuit potential in the frequency range 100 kHz to 0.01 Hz. All impedance data were fitted to appropriate circuits using the computer program Echem Analyst 5.0.

2.4. Gravimetric measurement

Gravimetric experiments were performed according to the standard methods [5]. Triplicate experiments have been done and the corrosion rates C_R (mm/y) were calculated from the following equation [6]:

$$C_R (\text{mm/y}) = \frac{87.6 \times w}{AtD} \quad (1)$$

where w is the average weight loss (in mg) of three parallel mild steel coupons, A the total area of one mild coupon, t is immersion time (h) and D the density of mild steel (gcm^{-3}). With the calculated corrosion rate, the inhibition efficiency $\eta\%$ was calculated as follows [6]:

$$\eta\% = \frac{w_0 - w_i}{w_0} \times 100 \tag{2}$$

where w_0 and w_i are the values of the corrosion weight losses of mild steel in absence and presence of inhibitors, respectively.

2.5. Surface characterization

The SEM analyses of mild steel coupons ($2.5 \times 2 \times 0.025$ cm) after abrading and immersion in 1M HCl in the absence and presence of optimum concentration (200 mgL^{-1}) of APTT was performed on a Ziess Evo 50 XVP instrument at an accelerating voltage of 5 kV and 5 K X magnification. Chemical composition of the corrosion products was recorded by an EDX detector.

3. RESULTS AND DISCUSSION

3.1. Electrochemical measurements

3.1.1. Open circuit potential (OCP) vs. time

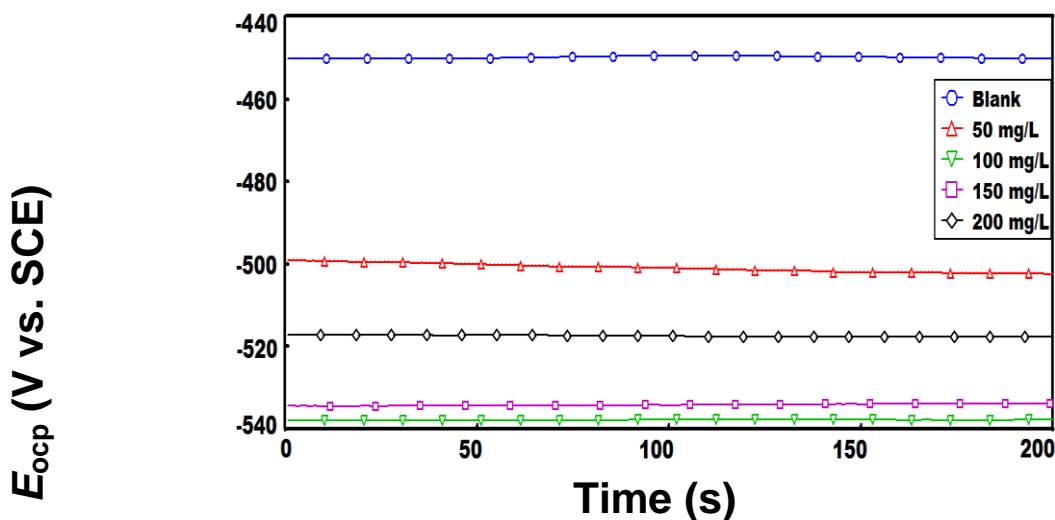


Figure 2. OCP curves for mild steel in 1M HCl in absence and presence of various concentrations of APTT at 308 K

The OCP is the potential of working electrode with respect to reference electrode without applied potential or current. It is required to maintain the stability of OCP before running the

polarization and EIS experiments. Fig. 2 shows the variation of OCP of working electrode with time in uninhibited and inhibited system at 308 K. The steady-state value of OCP is more negative than the immersion potential (E_{ocp} at $t=0$) in uninhibited solution suggest the dissolution of pre-immersion air formed oxide film on mild steel surface before the steady-state condition is achieved. This steady-state potential, which achieved quickly (for 30 min immersion) correspond to free corrosion of bare metal [7].

It is clear from Fig. 2 that addition of APTT to 1M HCl solution shifts the steady-state potential to more negative values without changing the general features of $E-t$ curves suggesting that they catalyze the dissolution of oxide film. The shift of OCP can be explained in terms of formation of protective inhibitor film on metal surface.

3.1.2. Potentiodynamic polarization

Polarization curves for mild steel in 1M HCl with APTT at different concentrations is shown in Fig. 3. The anodic and cathodic current–potential curves were extrapolated up to their intersection at the point where corrosion current density (I_{corr}) and corrosion potential (E_{corr}) were obtained. The electrochemical parameters E_{corr} , I_{corr} , anodic and cathodic Tafel slopes (b_a , b_c) obtained from the polarization measurements are listed in Table 1.

Table 1. Electrochemical polarization parameters for mild steel in 1M HCl solution in the absence and presence of different concentrations of APTT

C _{inh} (mg/L)	E _{corr} (mV/SCE)	I _{corr} (μ A/cm ²)	b _a (mV/dec)	b _c (mV/dec)	η (%)
Blank	-444	892	61.0	81.0	–
50	-519	204	45.9	132.0	81.4
100	-494	183	41.1	115.5	83.3
150	-517	97	47.7	131.3	91.1
200	-501	59	47.5	139.3	94.6

The percentage of inhibition efficiency (η %) was calculated using following equation [8] :

$$\eta\% = \left(1 - \frac{I_{corr(i)}}{I_{corr}} \right) \times 100 \quad (3)$$

where I_{corr} and $I_{corr(i)}$ are the uninhibited and inhibited corrosion current densities, respectively. The parallel cathodic Tafel curves in Fig. 3 suggested that the hydrogen evolution was activation-controlled and the reduction mechanism was not affected by the presence of the inhibitor.

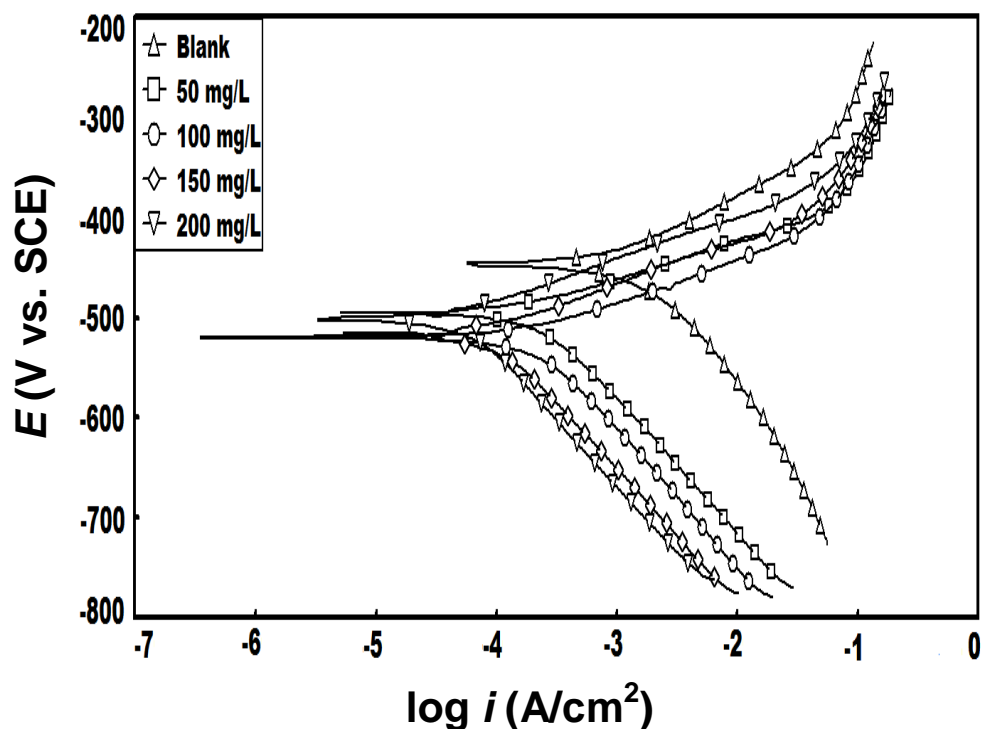


Figure 3. Potentiodynamic polarization curves for mild steel in 1M HCl in absence and presence of various concentrations of APTT at 308 K

The values of b_c changed significantly with increasing inhibitor concentrations, which indicated the effect of the compound on the kinetics of hydrogen evolution [9]. Compared with the blank, the anodic curves of the working electrode in the acid solution containing APTT shifted obviously to the direction of the current reduction, which implied that the organic compounds could also suppress the anodic reaction. Only as the change in E_{corr} value was more than 85 mV, a compound could be recognized as an anodic or a cathodic type inhibitor [10]. The largest displacement of E_{corr} was about 75 mV (Table 1). Therefore, APTT might act as a mixed-type inhibitor. Corrosion is an electrochemical phenomenon and inhibitors decrease the velocity of electrochemical electrode reactions. A lower I_{corr} value for inhibitor solutions implies that the rate of electrochemical reactions was reduced due to the formation of a barrier layer over the mild steel surface by the inhibitor molecules [11].

3.1.2. Electrochemical impedance spectroscopy

Electrochemical impedance spectroscopy is a significant method for investigation of protective properties of organic inhibitors on metals. The Nyquist plots obtained for mild steel in 1M HCl in the absence and presence of various concentrations of the APTT are shown in Fig.4. These plots were characterized by one depressed semicircular capacitive loop in the given frequency zone. The capacitive loop is related to the charge transfer process of the metal corrosion and the double layer

behavior, which is connected with the adsorption process of the APTT on the metal surface which increased with the increase of the inhibitor concentrations [12].

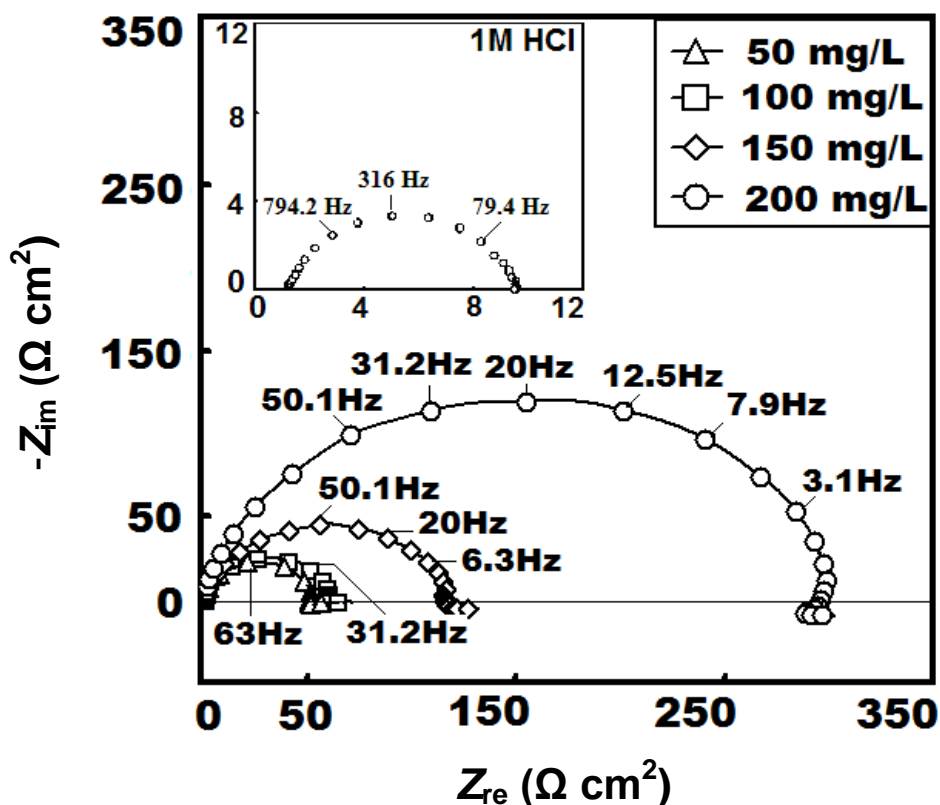


Figure 4. Nyquist plots for mild steel in 1M HCl in absence and presence of various concentrations of APTT at 308 K

The radius of the capacitive loop enlarged gradually with increasing concentrations of the inhibitor, indicating that the impedance of mild steel increases due to increasing surface coverage of electrode surface with adsorption of inhibitor molecules, consequently leading to an increase in the inhibition efficiency. The values of percentage inhibition efficiency (η %) were calculated from equation [13] :

$$\eta\% = \left(1 - \frac{R_{ct}}{R_{ct(i)}}\right) \times 100 \tag{4}$$

where $R_{ct(i)}$ and R_{ct} are the charge transfer resistance in presence and absence of APTT.

All the impedance parameters were calculated with the application of the equivalent circuit model Fig. 5 and listed in Table 2.

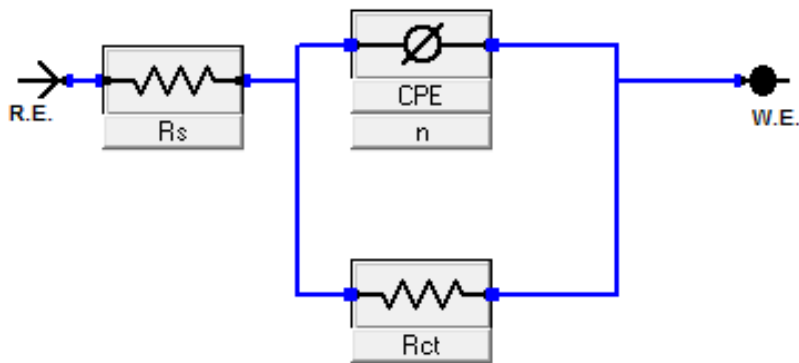


Figure 5. Equivalent circuit used to fit the EIS data

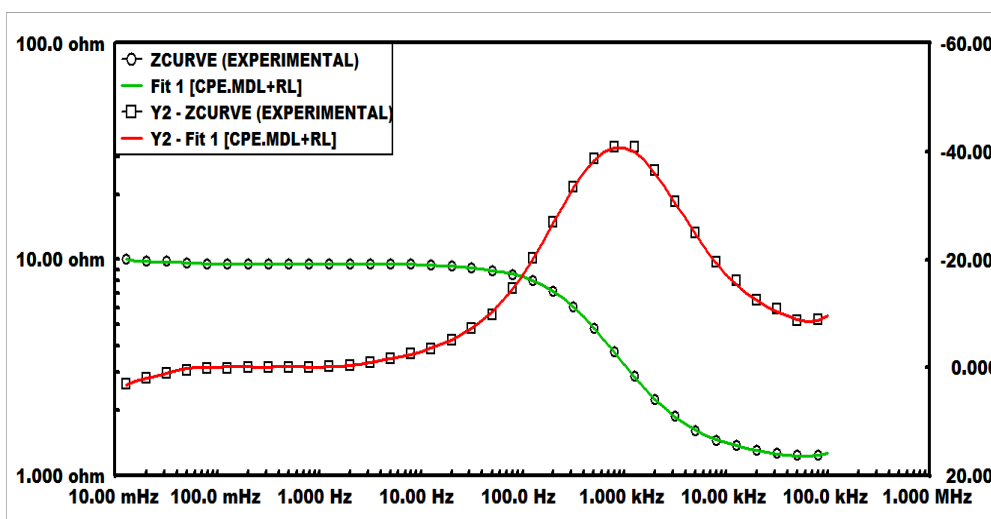


Figure 6. Simulated and experimentally generated Bode phase angle plots

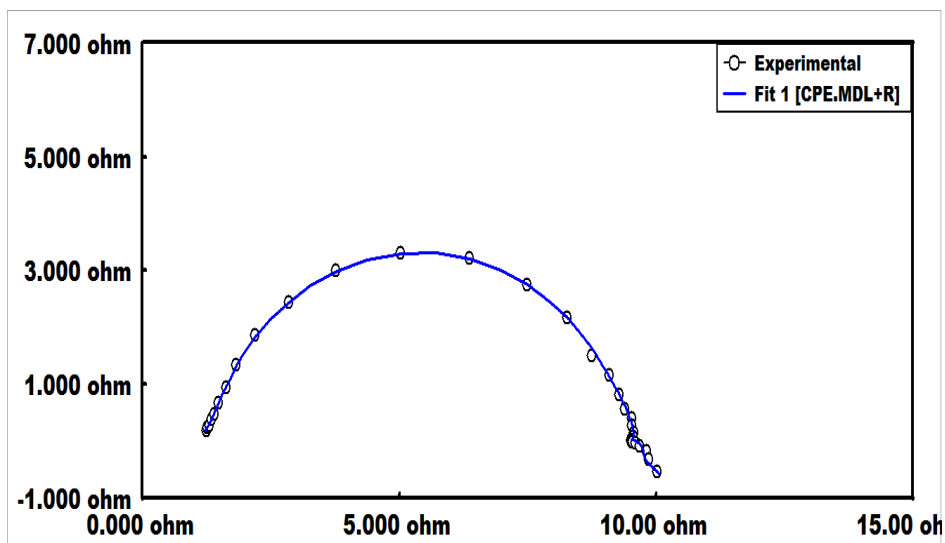


Figure 7. Simulated and experimentally generated Nyquist plot

This circuit consists of R_s (the resistance of solution between working electrode and counter electrode) C_{dl} in parallel to the R_{ct} . Simulation of Bode phase angle plots and Nyquist plot with above model showed excellent agreement with experimental data (Fig. 6 , 7). It should be noticed that the depression of the large semicircles which are not perfect semicircles in the complex impedance plane of the Nyquist plots (Fig. 4).

Deviation of this kind, often referred to as frequency dispersion, was attributed to roughness and inhomogeneity of the solid surface. Therefore, a constant phase element (CPE) instead of a capacitive element is used in Fig. 5 to get a more accurate fit of experimental data. The impedance, Z , of CPE has the form [13]:

$$Z_{CPE} = \left(\frac{1}{Y_0} \right) [(j\omega)_n]^{-1} \tag{5}$$

where Y_0 is the CPE constant, which is a combination of properties related to the surface and electro active species, $j^2 = -1$ the imaginary number, ω the angular frequency and n is a CPE exponent which can be used as a measure of the heterogeneity or roughness of the surface. Depending on the value of n , CPE can represent resistance ($n = 0, Y_0 = R$), capacitance ($n = 1, Y_0 = C$), inductance ($n = -1, Y_0 = L$) or Warburg impedance ($n = 0.5, Y_0 = W$) [14].

The values of double layer capacitance, C_{dl} , for a circuit including CPE were calculated according to following equation [14]:

$$C_{dl} = Y_0 (\omega_{max})^{n-1} \tag{6}$$

Table 2. Electrochemical impedance parameters for mild steel in 1M HCl solution in the absence and presence of different concentrations of APTT

Cinh (mgL-1)	Rs (Ω)	Rct (Ω cm2)	n	Y0 (μF/cm2)	Cdl (μF/cm2)	η (%)
Blank	0.580	12.98	0.79	250.1	109.5	-
50	0.703	52.11	0.90	89.8	53.4	76.1
100	0.952	59.33	0.88	52.0	34.8	79.0
150	0.900	119.4	0.85	64.8	24.2	89.6
200	0.873	296.5	0.88	43.8	22.5	95.8

Inspection of Table 2 reveals that R_{ct} values increases prominently while C_{dl} reduces with the concentration of APTT. A large charge transfer resistance is associated with a slower corroding system. In contrast, better protection provided by an inhibitor can be associated with a decrease in capacitance of the metal.

The decrease in C_{dl} comparing with that in blank solution (without inhibitor), which can result from a decrease in local dielectric constant and/or an increase in the thickness of the electrical double layer, suggests that the inhibitor molecules function by adsorption at the metal/solution interface [15].

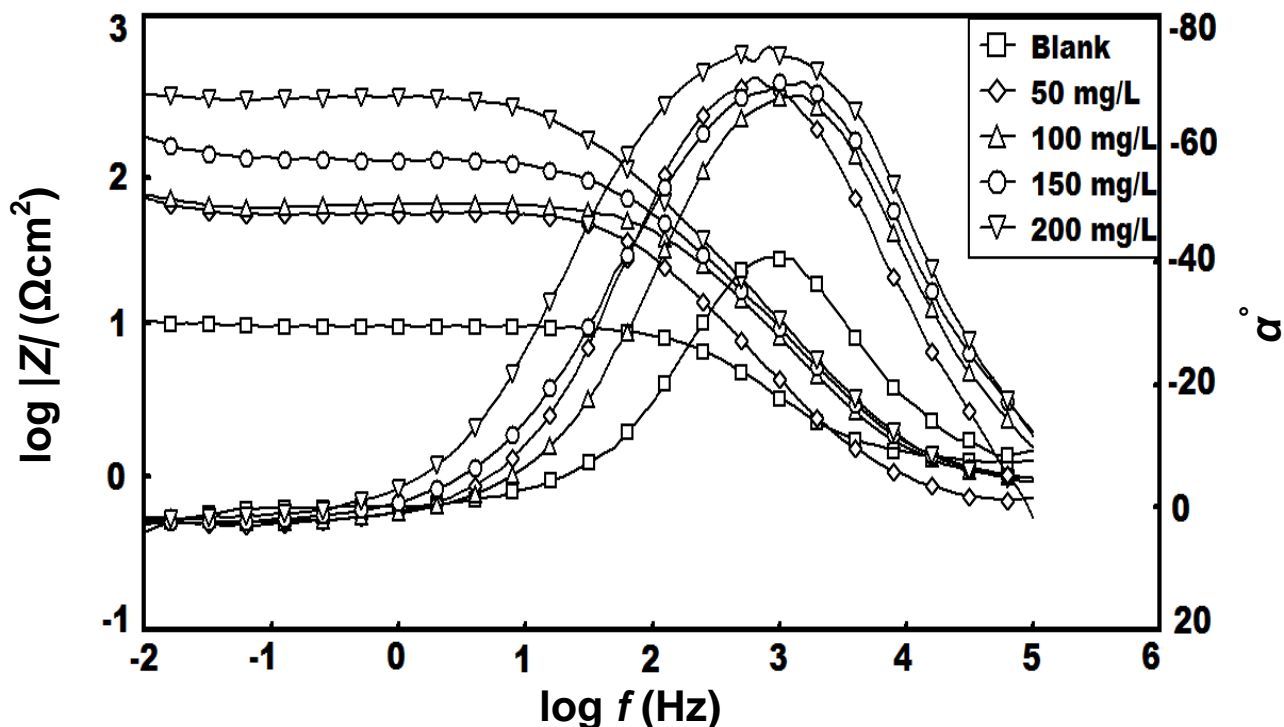


Figure 8. Bode ($\log f$ vs. $\log |Z|$) and phase angle ($\log f$ vs. α) plots of impedance spectra for mild steel in 1M HCl in absence and presence of various concentrations of APTT at 308 K

However, more adsorption of inhibitor molecules on metal surface, more the thickness of barrier layer is increased according to the expression of Helmholtz model [16]:

$$C_{dl} = \frac{\epsilon\epsilon_0}{d} S \tag{7}$$

where ϵ_0 is the permittivity of free space ($8.854 \times 10^{-12} \text{ Fm}^{-1}$) and ϵ is the local dielectric constant of medium, S is the surface area of the electrode. Equation (17) suggests that C_{dl} is inversely proportional to the thickness of protective layer d .

Fig. 8 shows the Bode phase angle plots recorded for mild steel electrode immersed in 1M HCl in the absence and presence of various concentrations of APTT at its open circuit potential. The values of Bode impedance magnitude (S) and maximum phase angles (α°) are listed in Table 3.

Table 3. The slopes of the Bode impedance magnitude plots at intermediate frequencies (S) and the maximum phase angles (α) for mild steel in 1M HCl solution at different concentrations of APTT at 308 K

C _{inh} (mgL ⁻¹)	- S	- α°
Blank	0.502	40.90
50	0.825	70.01
100	0.793	67.16
150	0.781	69.57
200	0.843	75.95

In the intermediate frequency region, a linear relationship between $\log |Z|$ against $\log f$, with slope near -1 and the phase angle tends to become -90° , can be observed. This response is a characteristic of capacitive behavior. An ideal capacitive response would result in a slope of -1 and a phase angle of -90° ; however, it is well known that an electrochemical system generally does not behave in an ideal manner [17]. In our case, in intermediate frequencies region, a linear relationship between $\log |Z|$ vs. $\log f$ with a slope near -0.84 and the phase angle approaching -80° has been observed. These deviations considered to be the deviation from the ideal capacitive behavior at intermediate frequencies. The Bode phase angle plots show single maximum (one time constant) at intermediate frequencies, broadening of this maximum in presence of APTT account for the formation of a protective layer on electrode surface [14].

3.2. Gravimetric measurements

3.2.1. Effect of inhibitor concentration

The values of percentage inhibition efficiency (η %) and corrosion rate (C_R) obtained from gravimetric method at different concentrations of APTT at 308 K are summarized in Table 4.

Table 4. Corrosion parameters obtained from gravimetric measurement for mild steel in 1M HCl in absence of presence of different concentrations of APTT at 308 K

C _{inh} (mg/L)	C _R (mm/year)	θ	η (%)
Blank	77.9	-	-
50	35.6	0.54	54.3
100	21.1	0.72	72.9
150	7.4	0.90	90.5
200	3.3	0.95	95.7

It has been found that inhibition efficiency of APTT increases with increase in concentration. The maximum inhibition efficiency was obtained at 200 mg L⁻¹ and further increase in concentration did not cause any appreciable change in the performance of inhibitor. The corrosion rate values decreases and inhibition efficiency increases.

3.2.2. Investigation of temperature effect

The influence of temperature on percentage inhibition efficiency was studied by conducting gravimetric measurements at 308-338 K containing optimum concentration of APTT. The values of corrosion rate in the studied temperature range are listed in Table 5.

Table 5. Corrosion parameters obtained from gravimetric measurement for mild steel in 1M HCl in presence of optimum concentration (200 mg L⁻¹) of APTT at different temperatures

Temperature (K)	1M HCl	APTT		
	CR (mm/year)	CR (mm/year)	θ	η (%)
308	77.9	3.31	0.95	95.7
318	107.6	16.7	0.84	84.5
328	162.5	58.6	0.64	64.0
338	208.5	111.3	0.46	46.6

It is clear from the Table 5 that the decrease in inhibition efficiency and increase in corrosion rate with increase in temperature may be probably due to increased rate of desorption of APTT from the mild steel surface at higher temperature [18].

The relationship between the corrosion rate (C_R) of mild steel in acidic media and temperature (T) is often expressed by the Arrhenius equation [19]:

$$\log(C_R) = \log A - \frac{E_a}{2.303RT} \quad (8)$$

where E_a is the apparent activation energy, R is the molar gas constant (8.314 J K⁻¹ mol⁻¹), T is the absolute temperature and A is the frequency factor. The plot of $\log(C_R)$ against $1/T$ for mild steel corrosion in 1M HCl in absence and presence of APTT is presented in Fig. 9. All parameters are listed in Table 6.

Table 6. Activation parameters for mild steel dissolution in 1M HCl in the absence and presence of optimum concentration of APTT

Inhibitors	Ea (kJ mol ⁻¹)	ΔH* (kJ mol ⁻¹)	ΔS* (J K ⁻¹ mol ⁻¹)
Blank	27.9	25.4	-147.4
APTT	124	121	155.11

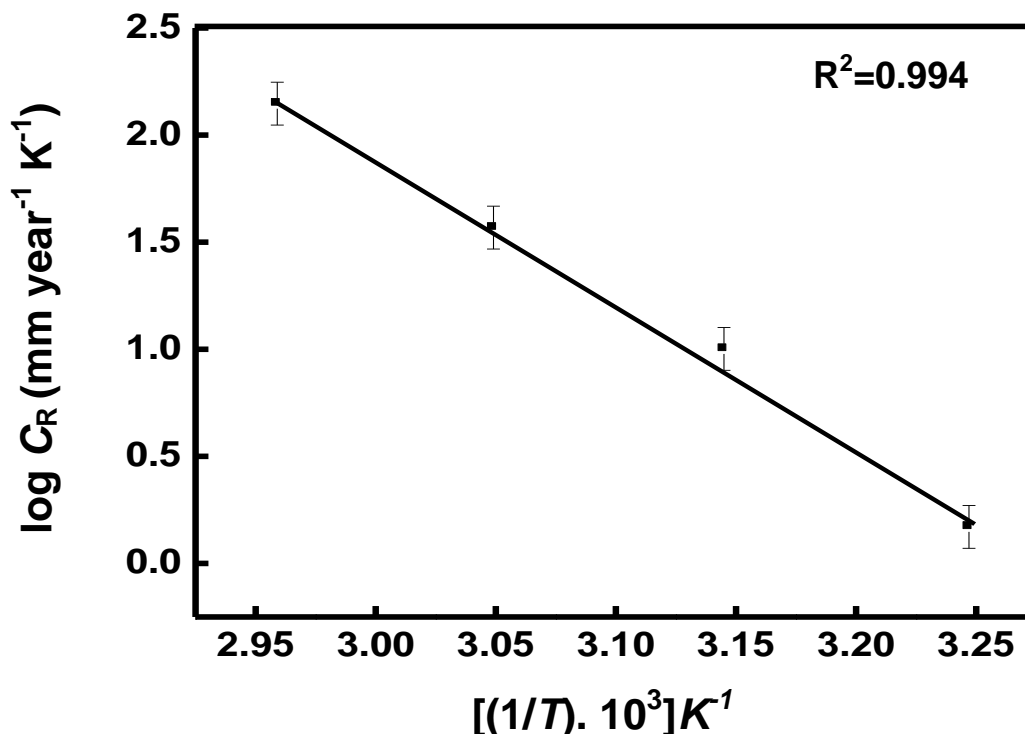


Figure 9. Arrhenius plot of mild steel in 1M HCl in absence and presence of optimum concentration of APTT

The increase in activation energy after the addition of the inhibitor (124 kJ mol⁻¹) to the uninhibited solution (27.9 kJ mol⁻¹) indicates that physical adsorption occurs in the initial stage. The higher E_a value in the inhibited solution can be correlated with the increased thickness of the double layer, which enhances the activation energy of the corrosion process [19].

Experimental corrosion rate values obtained from gravimetric measurements for mild in 1M HCl in the absence and presence of APTT was used to further gain insight on the change of enthalpy (ΔH*) and entropy (ΔS*) of activation for the formation of the activation complex in the transition state using transition state equation [20]:

$$C_R = \frac{RT}{Nh} \exp\left(\frac{\Delta S_a}{R}\right) \exp\left(-\frac{H_a}{RT}\right) \tag{9}$$

where h is the Plank's constant (6.626×10^{-34} Js), N is the Avogadro's number (6.022×10^{23} mol⁻¹), R is the universal gas constant and T is the absolute temperature. Fig. 10 shows the plot of $\log C_R / T$ versus $1/T$ for mild steel corrosion in 1M HCl in the absence and presence of APTT. Straight line is obtained with slope of $(\Delta H^*/2.303 R)$ and an intercept of $[\log (R/ Nh) + (\Delta S^* /2.303R)]$ from which the values of ΔH^* and ΔS^* respectively were computed and listed also in Table 6.

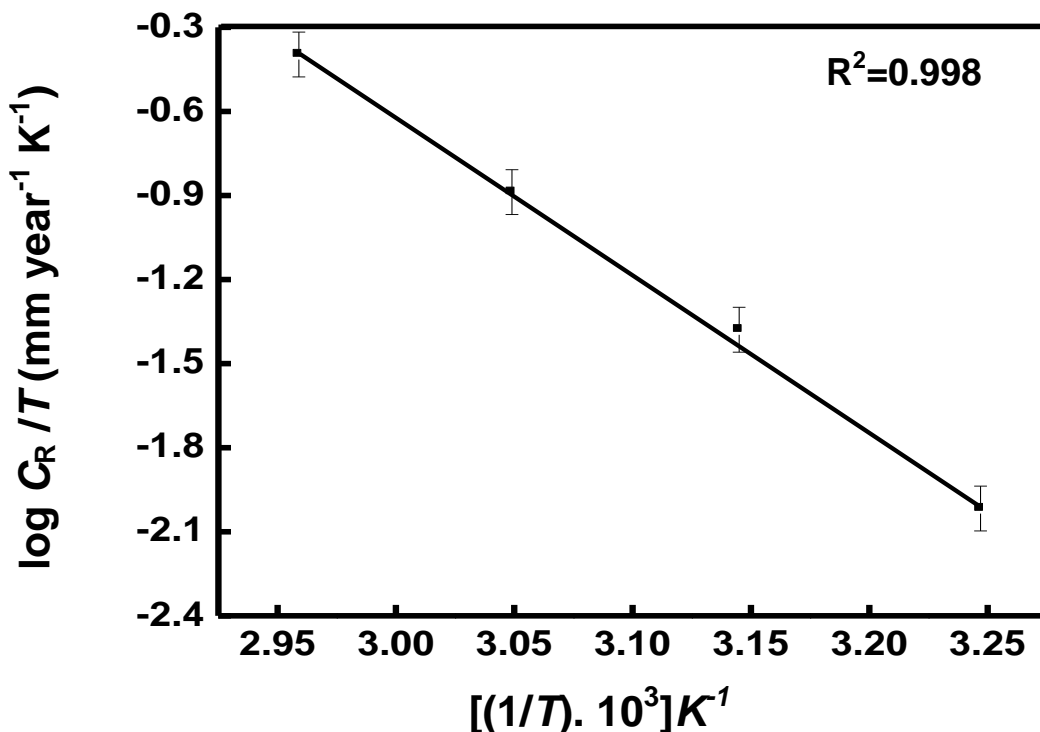


Figure 10. Transition-state plot of mild steel in 1M HCl in absence and presence of optimum concentration of APTT

The positive sign of ΔH^* suggests the endothermic nature of the mild steel dissolution process. The value of ΔS^* is higher for inhibited solution than that for the uninhibited solution. This suggested that an increase in randomness occurred on going from reactants to the activated complex. This might be results of the adsorption of APTT molecules from the acid solution could be regarded as quasi-substitution between the APTT in the aqueous phase and H₂O molecules on electrode surface. In such condition, the adsorption of APTT molecules was accompanied with desorption of H₂O molecules from the electrode surface. Thus increase in entropy of activation was attributed to solvent (H₂O) entropy [14].

3.2.3. Adsorption investigations

Basic information on the interaction between inhibitor and steel surface can be provided by the adsorption isotherm.

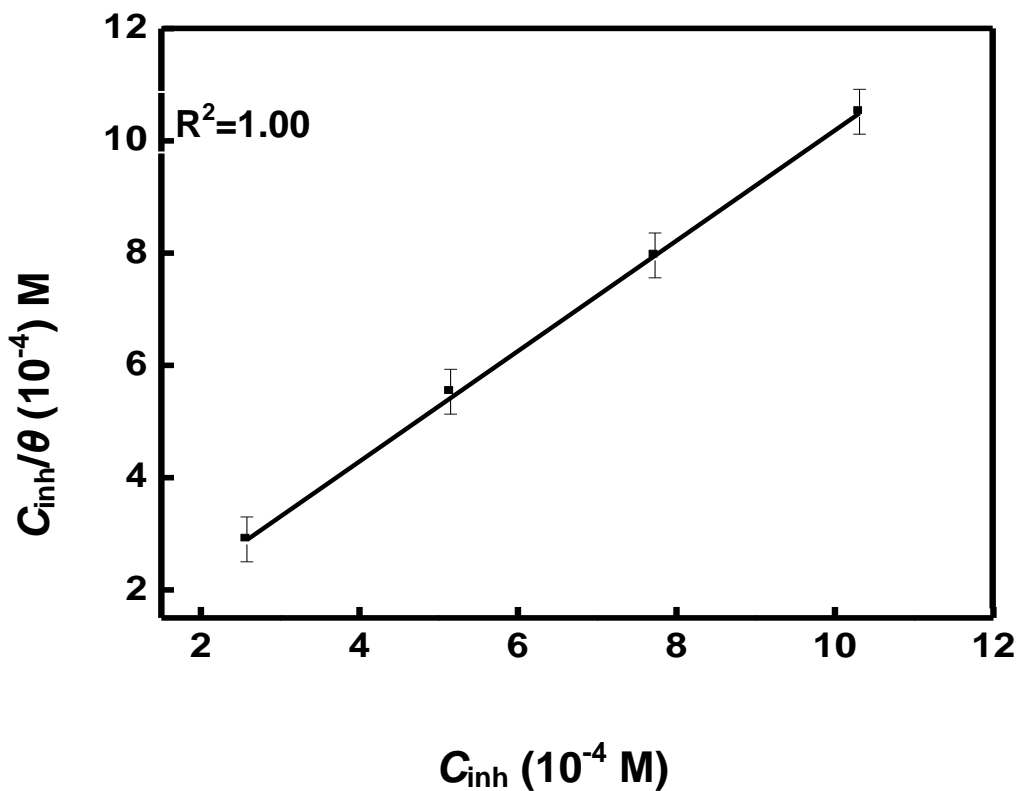


Figure 11. Langmuir’s isotherm for adsorption of APTT on mild steel surface in 1M HCl

Attempts were made to fit to various isotherms including Frumkin, Langmuir, and Temkin isotherms. By far the results are best fitted by Langmuir adsorption isotherm [21]:

$$\frac{C}{\theta} = \frac{1}{K_{ads}} + C \tag{10}$$

where C is the concentration of inhibitor (M), K_{ads} the adsorptive equilibrium constant (M^{-1}) and θ is the surface coverage which can be calculated by the following equation [21]:

$$\theta = \frac{w_0 - w_i}{w_0} \tag{11}$$

By plotting C/θ versus C at 308 K, straight line is obtained as seen in Fig. 11. The linear relationships ($R^2=1.00$) suggest that the adsorption of APTT obeys the Langmuir adsorption isotherm.

On the other hand, K_{ads} is also related to free energy of adsorption (ΔG°_{ads}) by the equation:

$$K_{ads} = \frac{1}{55.5} \exp\left(\frac{-\Delta G^\circ_{ads}}{RT}\right) \tag{12}$$

where R is the gas constant and T is the absolute temperature. The value of 55.5 is the concentration of water in solution in mol L^{-1} . The values of K_{ads} and $\Delta G^{\circ}_{\text{ads}}$ are listed in Table 7.

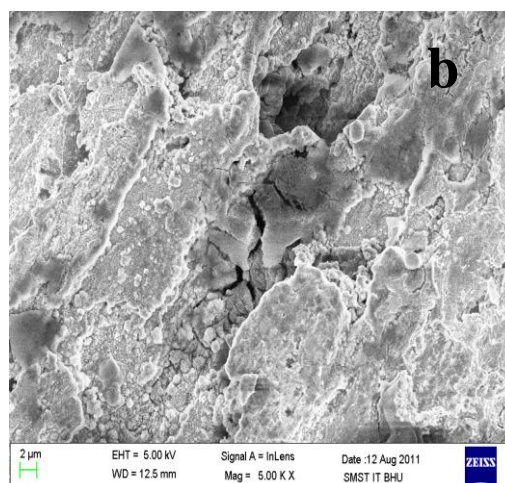
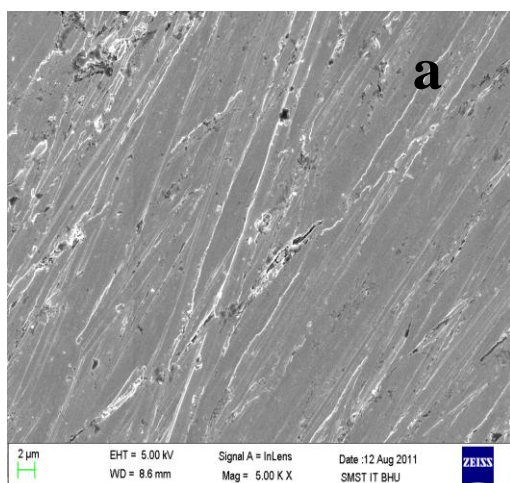
Table 7. Thermodynamic parameters for the adsorption of APTT on mild steel in 1M HCl at different temperatures

Temperature (K)	K_{ads} (10^3 M^{-1})	$\Delta G^{\circ}_{\text{ads}}$ (kJ mol^{-1})
308	58.8	-38.42
318	6.49	-33.84
328	2.12	-31.86
338	1.04	-30.84

The calculated values of $\Delta G^{\circ}_{\text{ads}}$ for studied inhibitors were ranging from -30 to -39 kJmol^{-1} which indicated that adsorption of APTT on the mild steel surface may involve physical as well as chemical adsorption and the decrease in values of K_{ads} with increasing temperature suggested that the desorption process enhances with elevating temperature [22].

3.3. SEM and EDX

The surface morphology of the mild steel before immersion in 1M HCl showed a freshly abraded steel surface (Fig. 12a), abrading scratches are clearly visible on the surface. SEM images of mild steel surface after immersion in 1M HCl for 3 h in the absence and presence of optimum concentration of APTT are shown in Fig. 12b and 12c, respectively. It could be observed from Fig. 12b that the specimen surface was strongly damaged in the absence of the inhibitor. SEM image of the mild steel surface after immersion in 1M HCl with optimum concentration of APTT is shown in Fig. 12c, it could be seen that in presence of the inhibitor, the rate of corrosion was suppressed, it revealed that there was a good protective film adsorbed on metal surface, which was responsible for the inhibition of corrosion.



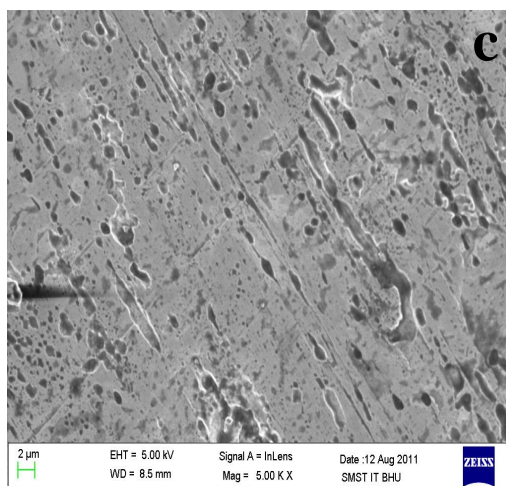


Figure 12. SEM micrographs of mild steel surfaces (a) abraded mild steel (b) uninhibited 1M HCl (c) APTT

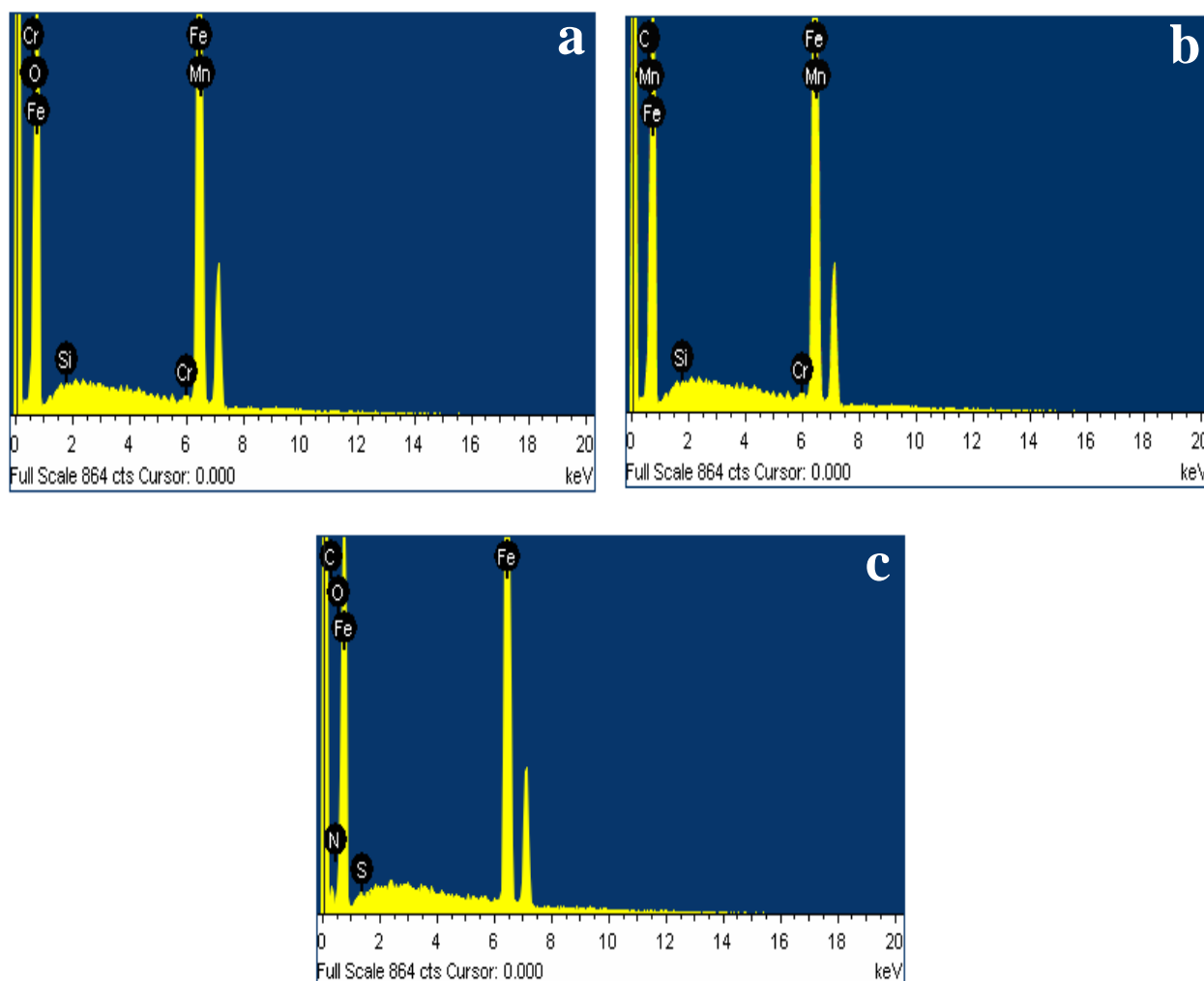


Figure 13. EDX spectra of mild steel specimens (a) abraded mild steel (b) uninhibited 1M HCl (c) APTT

Fig. 13 a-c presents EDX spectra recorded for mild steel specimen as those used for SEM. For mild steel before immersion in 1M HCl (Fig. 13a), the spectrum shows the characteristics peaks of some of the elements constituting the mild steel sample. Fig. 13b is the EDX spectrum of uninhibited mild steel sample, the peak of O is absent which confirm the dissolution of air formed oxide film and free corrosion of bare metal as described in OCP measurements. The EDX spectrum of mild steel specimen in presence of APTT (Fig. 13c) shows additional lines characteristic for the existence of N and S (due to the N and S atoms of the APTT). These observations confirm the presence of protective film of inhibitor on electrode surface. The percentage atomic content of mild steel samples obtained from EDX analyses is listed in Table 8.

Table 8. Percentage atomic contents of elements obtained from EDX spectra

	Fe	C	Si	Mn	Cr	N	O	S
Polished mild steel	70.3	28.0	0.23	0.34	0.44	-	0.69	-
Blank	63.9	36.1	-	0.24	-	-	-	-
APTT	65.3	30.7	-	-	-	1.77	1.23	1.00

3.4. Explanation of Inhibition

The inhibition mechanism can be proposed from the adsorption of inhibitor on steel surface (Fig. 14). Thus, in acid solution the studied inhibitor exist as protonated species. The charge on the metal surface can be determined from the value of $E_{corr} - E_{q=0}$ (zero charge potential). The $E_{q=0}$ of iron is -530 mV vs. SCE in HCl [23]. In our investigation, the value of E_{corr} obtained in 1M HCl is -444 mV vs. SCE. So, the steel surface charges positive in HCl solution because of $E_{corr} - E_{q=0} > 0$.

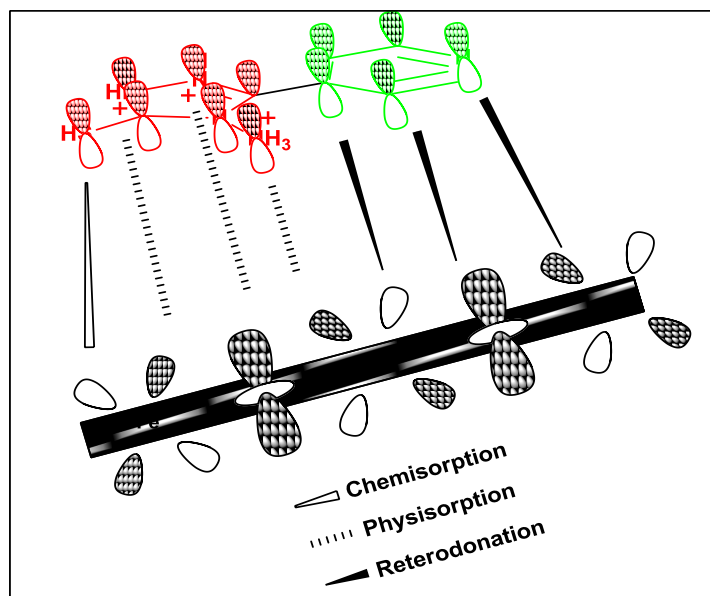


Figure 14. Schematic adsorption mode of APTT molecule on mild steel surface in 1M HCl

Since Cl^- ions are already adsorbed on the metal surface hence they favor more adsorption of protonated inhibitor on metal surface through electrostatic interaction (Physisorption). The physically adsorbed protonated forms of APTT molecules in acid medium start competing with H^+ ions for electrons on mild steel surface. After release of H_2 gas, protonated form of inhibitors returns to its neutral form and heteroatoms with free lone pair electrons promote chemical adsorption [24]. The accumulation of electrons on mild steel surface render it more negative and to relieve the metal from extra negative charge the electron from d-orbital of Fe might be transferred to vacant π^* (antibonding) orbital of inhibitor molecules (reterodonation) and hence strengthen adsorption on metal surface.

4. CONCLUSION

APTT was found to inhibit the corrosion of mild steel in 1M HCl solution and the extent of inhibition was concentration dependent. Inhibition efficiency increases with increasing inhibitor concentration. Polarization curves proved that APTT is a mixed-type inhibitor, which can suppress anodic and cathodic reactions at the same time. EIS plots indicated that the inhibitor increases the charge-transfer resistances and showed that the inhibitive performance depends on adsorption of the molecule on the metal surface. The adsorption of APTT on mild steel surface is found to obey the Langmuir adsorption isotherm. The SEM and EDX analysis showed that the addition of inhibitors to the corrosive solutions results through the formation of protective film on mild steel surface.

ACKNOWLEDGEMENT

Council of Scientific and Industrial Research (CSIR), New Delhi, India, is gratefully acknowledged for the financial assistance.

References

1. E. Naderi, A. H. Jafari, M. Ehteshamzadeh and M.G. Hosseini, *Mater. Chem. Phys.* 115 (2009) 852
2. Y. Abbouda, A. Abourrichea, T. Saffaja, M. Berradaa, M. Charroufa, A. Bennamaraa and H. Hannache, *Desalin.* 237 (2009) 175
3. M.J. Bahrami, S.M.A. Hosseini and P. Pilvar, *Corros. Sci.* 52 (2010) 2793
4. Y. Murti, R. Agnihotri and D. Pathak, *Am. J. Chem.* 1(2) (2011) 42
5. ASTM (1990), "Standard practice for laboratory immersion corrosion testing of metals", Annual Book of Standards, G 31-72, American Society for Testing and Materials, Philadelphia, PA.
6. I. Ahamad, R. Prasad and M.A. Quraishi, *Corros. Sci.* 52 (2010) 933
7. H.H. Hasan, E. Abdelghani, M.A. Amin, *Electrochim. Acta.* 52 (2007) 6359
8. K. F. Khaled, *Electrochim. Acta.* 54 (2009) 6523
9. W. Li, Q. He, C. Pei, B. Hou, *Electrochim. Acta.* 52 (2007) 639
10. H. Ashassi-Sorkhabi, M.R. Majidi and K. Seyyedi, *Appl. Surf. Sci.* 225 (2004) 176
11. K. S. Jacob and G. Parameswaran, *Corros. Sci.* 52 (2010) 224
12. M. Outirite, M. Lagrenée, M. Lebrini, M. Traisnel, C. Jama, H. Vezin and F. Bentiss, *Electrochim. Acta.* 55 (2010) 1670
13. E. Machnikova, K. H. Whitmire and N. Hackerman, *Electrochim. Acta.* 53 (2008) 6024
14. D. K. Yadav, M. A. Quraishi and B. Maiti, *Corros. Sci.* 55 (2012) 254
15. A.Y. Musa, R.T.T. Jalgham and A. B. Mohamad, *Corros. Sci.* 56 (2012) 176

16. K. Singh and M.A. Quraishi, *Corros. Sci.* 52 (2010) 1373
17. H. H. Hassan, *Electrochim. Acta.* 53 (2007) 1722
18. X. Li, S. Deng and H. Fu, *Prog. Org. Coat.* 67 (2010) 420
19. N. Soltani, M. Behpour, S.M. Ghoreishi and H. Naeimi, *Corros. Sci.* 52 (2010) 1351
20. A.Singh, I. Ahamad, D. K. Yadav, V. K. Singh and M. A. Quraishi, *Chem. Eng. Comm.* 199 (2012) 63
21. X. Li, S. Deng and H. Fu, *Corros. Sci.* 55 (2012) 280
22. D. K. Yadav, B. Maiti and M. A. Quraishi, *Corros. Sci.* 52 (2010) 3586
23. S. Deng, X. Li and H. Fu, *Corros. Sci.* 53 (2011) 760
24. O. O. Xometi, N.V. Likhanova, M.A. D. Aguilar, E. Arcec, H. Dorantes and P. A. Lozadaa, *Mater. Chem. Phys.* 110 (2008) 344